Journal of Applied Electrochemistry **29**: 1035–1044, 1999.

Electrodeposition of zinc–nickel alloys from ammonia-containing baths

I. RODRIGUEZ-TORRES, G. VALENTIN and F. LAPICQUE*
Laboratoire des Sciences du Génie Chimique, CNRS-ENSIC-INPL, BP 451, F-54001 Nancy, France
*(*author for correspondence, e-mail: lapicque@ensic.u-nancy.fr; fax: +33 3 83322975)*

Received 22 June 1998; accepted in revised form 22 December 1998

Key words: ammonia, cyclic voltammetry, electrodeposition, gas–liquid equilibria, speciation diagrams, zinc–nickel alloys

Abstract

This paper describes the use of ammonia-containing baths for Zn–Ni alloy electrodeposition. Buffering properties of the ammonia/ammonium couple limit the local change in pH in the vicinity of the electrode surface caused by simultaneous hydrogen evolution. In addition, it is shown that the divalent zinc and nickel species exist in the form of $Zn(NH_3)_4^{2+}$ and $Ni(NH_3)_6^{2+}$ complexes over a large pH range. The electrochemistry of the deposition at pH 10 was investigated by galvanostatic experiments and cyclic voltammetry, and compared with deposition from ammonium chloride baths at pH 5. The Ni content in the alloys were found to be 40–60% higher from the ammonia-containing bath than from the acidic baths. Reduction of divalent ions and hydrogen evolution were shown to occur at potentials 250 mV more cathodic than with baths at pH 5; the deposition mechanism may be affected by complexation of the metal cations by ammonia.

1. Introduction

New coating processes have been developed for years for more efficient protection of steel plates or other metal pieces. Cadmium- and cadmium-based alloys of significant toxicity, have been replaced by other materials such as zinc- or nickel-containing alloys [1]. Development of zinc plating processes is, however, hindered by the moderate adherence of zinc on the substrate and its fair brittleness. Zinc–nickel and zinc–cobalt alloys present higher resistance to corrosion than pure zinc [2] and improved mechanical properties. In particular, Ni contents in the range 12–15 wt % in zinc alloys allow deposits with good coating properties, namely, excellent corrosion resistance [3] and reduced mechanical stresses. Such alloys can be used in automotive industry [4, 5] as for the production of engine compartments or in electronic industry [6].

In most cases zinc–nickel electrodeposition is an anomalous process according to Brenner's definition [7] since the content of nickel (the more noble metal) is appreciably lower in the deposit than in the electrolytic bath. The anomalous character of the deposition has been extensively investigated and amongst the various interpretations published, the mechanisms suggested by Wiart et al. [8–10] provide physical description of the existing interactions between zinc, nickel and hydrogen codepositions.

The properties of alloys result from their composition, as well as their structure and their morphology: all three depend on the process conditions such as temperature, current density and composition of the electrolytic bath. Zn–Ni alloys can be produced from various baths consisting of sulfate [1], chloride [11], acetate [12] and citrate [13] salts. The pH of electrolytic baths is a significant parameter since nickel and zinc cations form hydroxides at pH > 6. Also, the side evolution of hydrogen results in the local increase in pH, and the solid hydroxides formed are known to block the electrode surface. The addition of large amounts of ammonium chloride as a supporting electrolyte, reduces the increase in pH [3], [14, 15]. Moreover, the formation of hydroxides can be avoided using complexing agents such as cyanides [16] or amines [5] in fairly alkaline media.

This work aims at investigating the potential of ammonia-containing baths with alkaline pH. High pH are expected to allow fair Ni contents since zinc deposition is known to be favoured in acidic media [8, 9]; in addition the complexing properties of ammonia are to allow the existence of soluble complexes in a large pH range. Ammonia-containing baths have been investigated at pH 10, and at fixed concentrations of zinc and nickel chloride. Thermodynamic calculations yielded Zn and Ni speciation diagrams, indicating the nature of the metal species present in the electrolytic baths. The electrochemistry of alloy deposition from the alkaline media was investigated by cyclic voltammetry and galvanostatic runs at the surface of a platinum rotating disc electrode: the nickel contents and the (i/E) curves

were compared with those obtained from ammonium chloride baths at pH 5 with the same concentrations of metal salts.

2. Experimental details

Three chloride baths were prepared using conductimetry water and metal salts of analytical grade (Prolabo, France). For all cases, the concentrations of zinc and nickel chloride were fixed at 0.22 and 0.12 mol dm^{-3}, respectively. Two electrolytic baths were prepared with ammonium chloride (Prolabo, France) at 4 mol dm^{-3} as a supporting electrolyte. For both solutions the pH was adjusted to 5.0 by addition of chlorhydric acid or sodium hydroxide. Experiments were carried out in the presence of boric acid at 30 dm^{-3} or without boric acid. The alkaline bath was prepared with 0.6 mol dm^{-3} ammonium chloride and concentrated ammonia solution so that the total concentration of NH_3/NH_4^+ was 4 mol dm^{-3}. The alkaline solution with a pH at 10.0, was stored in a closed vessel to prevent from losses of ammonia vapour; a fresh alkaline bath was prepared for each experiment series. The compositions of the three electrolyte solutions used are reported in Table 1.

Experiments were conducted at a platinum RDE (EG&G, PAR 616) 4.0 mm diameter. Prior to measurements, the electrode surface was carefully polished with fine emery paper and diamond paste with successive grain sizes 6, 3 and 0.1 μm (Escil, Lyon, France), then rinsed in conductimetry water. All potentials were referred to the saturated calomel electrode (SCE) and were not corrected for ohmic drop. A sheet of Pt–Ti expanded metal was the counterelectrode. The electrodes were immersed in a 100 cm^3 glass cell covered by its cap and provided with a water jacket; the temperature was controlled at 25 °C. Voltammetric measurements at the motionless electrode and deposition runs at controlled current and rotation rate, were carried out using a EG&G 273 A potentiostat. Experimental (i/E) curves or time variations of the electrode potential were stored with a PC computer for interpretation and graphics. The deposits produced for galvanostatic runs were dissolved in 10 wt % nitric acid and the solutions obtained were analysed by atomic absorption with a spectrAA-20 (Varian, Paris, France).

Table 1. Chemical composition of the electrolytic baths used

Bath	Composition	pH
1	0.22 M $ZnCl_2$ + 0.12 M $NiCl_2.6\,H_2O$ + 4 M NH_4Cl	5
2	0.22 M $ZnCl_2$ + 0.12 M $NiCl_2.6\,H_2O$ + 4 M NH_4Cl + 30 g dm^{-3} H_3BO_3	5
3	0.22 M $ZnCl_2$ + 0.12 M $NiCl_2.6\,H_2O$ + 0.6 M NH_4Cl + 3.4 M NH_3	10

3. Thermodynamics of ammonia-containing solutions

3.1. *Speciation diagrams*

Speciation diagrams were calculated at 25 °C for the separate Zn(II)–NH_3–H_2O and Ni(II)–NH_3–H_2O systems to determine the operating conditions allowing the existence of soluble ammonia complexes of divalent metals. The solution pH was in the range 0–14. The concentrations of both metal species and ammonia were expressed by pMe and pNH_3', defined as the inverse of the logarithm of the total concentrations of metal species and ammonia-containing compounds, respectively. The metals considered were assumed to be introduced in the solution as chloride salts. Tables 2 and 3 give the equilibrium constants of the various equilibria involving zinc and nickel ions, respectively [17–21]. Ni^{2+} and Zn^{2+} ions when dissolved in a chloride medium, form complexes $NiCl^+$, $ZnCl^+$, $ZnCl_2$, $ZnCl_3^-$ and $ZnCl_4^{2-}$. The values of the formation constants of complexes $MCl_n^{(2-n)}$ from Cl^- and $MCl_{n-1}^{(3-n)}$ are of the order of 1 dm^3 mol^{-1} [20, 21], which is far below those of ammonia containing complexes. For simplicity, complexation processes of the metal ions by chloride were not taken into account in the present study. In addition, the nonideal behaviour of the solutions was neglected due the large number of species involved.

The speciation diagrams were established following the procedure suggested by Rojas et al. [22] and using the equilibrium constants together with the dissociation product of water at 10^{-14} mol^2 dm^{-6} at 25 °C. In the absence of ammonia, Zn^{2+} was shown to predominate in acidic or neutral solutions. $Zn(OH)_2$ form prevails in the range 8.8–11.5, $Zn(OH)_3^-$ exists in a narrow pH range, and $Zn(OH)_4^{2-}$ is the major species for pH over 12.1. Regardless of the likely formation of $NiCl^+$, divalent nickel is in the form of Ni^{2+} below pH 9.95. Over this pH limit hydroxides predominate: $Ni(OH)_2$ below 10.9, $Ni(OH)_3^-$ in the range 10.9–13.3 and

Table 2. Equilibrium constants of the various equilibria for the Zn(II)–NH_3–H_2O system

System	Equilibria	log K	Ref
Zn(II)–NH_3	$Zn^{2+} + NH_3 \rightarrow Zn(NH_3)^{2+}$	2.27	[17]
	$Zn^{2+} + 2\,NH_3 \rightarrow Zn(NH_3)_2^{2+}$	4.61	
	$Zn^{2+} + 3\,NH_3 \rightarrow Zn(NH_3)_3^{2+}$	7.01	
	$Zn^{2+} + 4\,NH_3 \rightarrow Zn(NH_3)_4^{2+}$	9.06	
H^+–NH_3	$NH_3 + H^+ \rightarrow NH_4^+$	9.27	[18]
Zn(II)–OH^-	$Zn^{2+} + OH^- \rightarrow Zn(OH)^+$	4.64	[18]
	$Zn^{2+} + 2\,OH^- \rightarrow Zn(OH)_{2(aq)}$	10.40	
	$Zn^{2+} + 3\,OH^- \rightarrow Zn(OH)_3^-$	12.93	
	$Zn^{2+} + 4\,OH^- \rightarrow Zn(OH)_4^{2-}$	14.82	
Zn(s)	$Zn^{2+} + 2\,OH^- \rightarrow Zn(OH)_{2(s)}$	15.60	[19]
Zn(II)–Cl^-	$Zn^{2+} + Cl^- \rightarrow ZnCl^+$	0.43	[20, 21]
	$ZnCl^+ + Cl^- \rightarrow ZnCl_2$	0.18	
	$ZnCl_2 + Cl^- \rightarrow ZnCl_3^-$	−0.09	
	$ZnCl_3^- + Cl^- \rightarrow ZnCl_4^{2-}$	−0.30	

Table 3. Equilibrium constants of the various equilibria for the Ni(II)–NH_3–H_2O system

System	Equilibria	log K	Ref
Ni(II)–NH_3	$Ni^{2+} + NH_3 \rightarrow Ni(NH_3)^{2+}$	2.75	[17]
	$Ni^{2+} + 2\ NH_3 \rightarrow Ni(NH_3)_2^{2+}$	4.95	
	$Ni^{2+} + 3\ NH_3 \rightarrow Ni(NH_3)_3^{2+}$	6.64	
	$Ni^{2+} + 4\ NH_3 \rightarrow Ni(NH_3)_4^{2+}$	7.79	
	$Ni^{2+} + 5\ NH_3 \rightarrow Ni(NH_3)_5^{2+}$	8.50	
	$Ni^{2+} + 6\ NH_3 \rightarrow Ni(NH_3)_6^{2+}$	8.49	
H^+–NH_3	$NH_3 + H^+ \rightarrow NH_4^+$	9.27	[18]
Ni(II)–OH^-	$Ni^{2+} + OH^- \rightarrow Ni(OH)^+$	3.58	[18]
	$Ni^{2+} + 2\ OH^- \rightarrow Ni(OH)_{2(aq)}$	8.10	
	$Ni^{2+} + 3\ OH^- \rightarrow Ni(OH)_3^-$	11.2	
	$Ni^{2+} + 4\ OH^- \rightarrow Ni(OH)_4^{2-}$	11.9	
Ni(s)	$Ni^{2+} + 2\ OH^- \rightarrow 2\ Ni(OH)_{2(s)}$	14.3	[19]
Ni(II)–Cl^-	$Zn^{2+} + Cl^- \rightarrow ZnCl^+$	0	[20, 21]

$Ni(OH)_4^{2-}$ in very alkaline media. The presence of single hydroxyl complexes $NiOH^+$ and $ZnOH^+$ seem unlikely due the equilibrium constants of their formation compared with those for the formation of $Ni(OH)_2$ and $Zn(OH)_2$: $NiOH^+$ and $ZnOH^+$ would exist for pH more alkaline than 10.42 and 9.36, respectively, whereas neutral $Ni(OH)_2$ and $Zn(OH)_2$ predominate at pH over 9.95 and 8.80. Besides and because of their low solubility, the neutral hydroxides are under dissolved state only for concentrations below 10^{-6} mol dm^{-3}.

Figure 1(a) and (b) shows the zone of predominant species depending on pH and pNH_3'. The diagrams were established regardless of the concentration of metal salts, and the two neutral hydroxides were considered to be under dissolved state. Due to the equilibrium constants of NH_3 complexes of zinc, only $Zn(NH_3)_3^{2+}$ and $Zn(NH_3)_4^{2+}$ were in significant concentrations and the presence of the two other complexes was therefore not considered (Figure 1(a)). For the example of 4 mol dm^{-3} ammonia-containing solutions (pNH_3' near -0.6), the diagrams show the existence of soluble NH_3 complexes for pH > 6.3 for zinc and pH 6.0 for nickel. The well-known complexes $Zn(NH_3)_4^{2+}$ and $Ni(NH_3)_6^{2+}$ mentioned for concentrated solutions of ammonia/ammonium solutions are the major forms of the metal salts for pH > 6.5 and 8.7, respectively. For the considered concentration of NH_3/NH_4^+ species, the complexes are stable in a broad pH range, and hydrated zincate ion prevails only for pH more alkaline than 13.2.

According to [19], zinc and nickel hydroxides are formed with metal concentrations at 10^{-3} mol dm^{-3} for pH > 7.3 and 8.3. The formation of insoluble hydroxides had therefore to be taken into account for the considered pNH_3' value. Figure 2(a) and (b) show the results depending on the overall concentration of metal species. For a 0.1 mol dm^{-3} solution, a free zinc cation was shown to predominate in acidic media for pH below 6.4, $Zn(NH_3)_3^{2+}$ exists in the narrow range 6.3–6.6, and the 4-ammonia complex is the major form for pH ranging from 6.6 to 13.1. Hydroxides $Zn(OH)_2$ (in solid

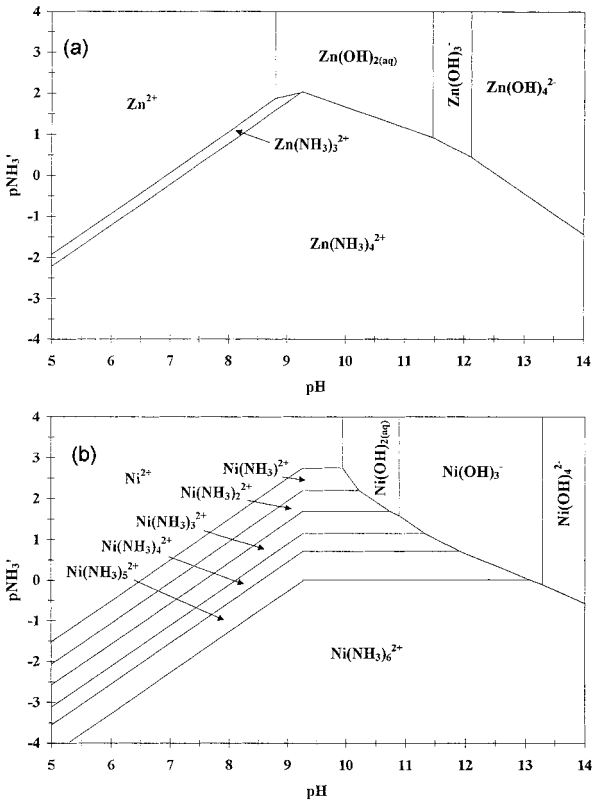

Fig. 1. Speciation diagrams at 25 °C: effects of pH and pNH_3'. (a) Zn(II)–NH_3–H_2O system, (b) Ni(II)–NH_3–H_2O system.

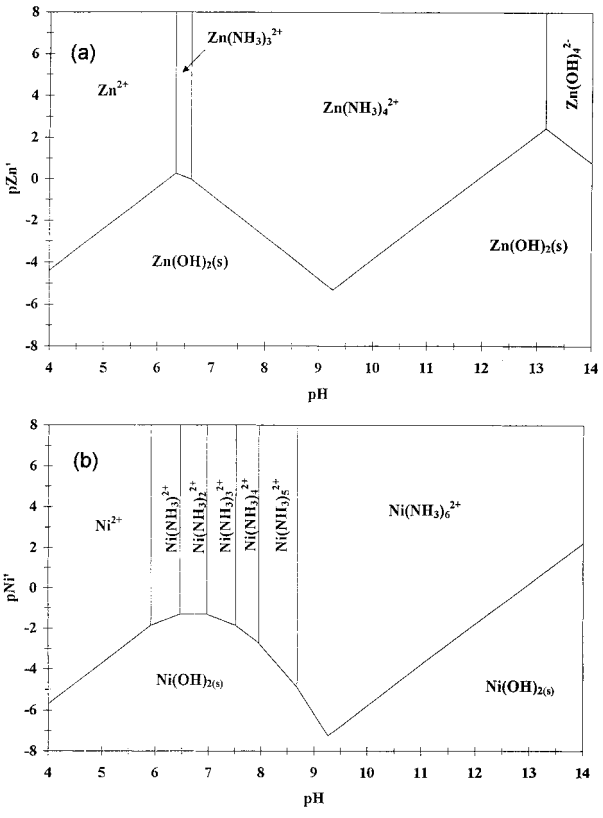

Fig. 2. Speciation diagrams with formation of insoluble $Me(OH)_2$ for $pNH_3' = -0.6$. (a) Zn(II)–NH_3–H_2O system, (b) Ni(II)–NH_3–H_2O system.

form) and $Zn(OH)_4^{2-}$ are only formed in concentrated alkaline solutions. For Ni(II) solutions at the same concentration, formation of $Ni(OH)_2$ occur only for pH > 13.4. Ammonia complexes of Ni(II) are formed for pH over 5.9 and the hexa-ammonia species predominates in the pH range 8.65–13.4.

To conclude, the above calculations show that divalent nickel and zinc are under soluble ammonia complexes over a large pH range. In addition, for the case of bath 3 with a large concentration of ammonia and a pH at 10, the metal species are mainly under the forms $Zn(NH_3)_4^{2+}$ and $Ni(NH_3)_6^{2+}$.

3.2. *Gas–liquid equilibrium*

The presence of molecular ammonia in the electrolytic solution is to result in significant vapour pressure in the gas phase. The partial pressure of ammonia in the gas phase over the electrolyte solutions was estimated by calculation of gas–liquid equilibria; the principle and the results obtained are reported in the Appendix. For bath 3 at 25 °C, the partial pressure of ammonia was found to be near 0.017 atm. Although Ni–Zn deposition is often carried out at temperatures over the ambient temperature to reduce the mechanical stresses in the deposit, the fair volatility of ammonia led us to fix the temperature at 25 °C.

4. Galvanostatic deposition of Ni–Zn alloy

Galvanostatic experiments were carried out at 1000 rpm for current densities varying from 10 to 280 mA cm^{-2}. The range of current density was chosen from estimates for the limiting current densities of metal deposition: assuming diffusion coefficients of the electroactive species at 5×10^{-10} m^2 s^{-1} and a viscosity at 10^{-6} m^2 s^{-1}, and taking into account the metal salt concentrations in the bath, the limiting current densities (c.d.'s) were estimated at 166 and 91 mA cm^{-2}, for the depositions of zinc and nickel, respectively. Assuming the two electroactive species diffuse independent of one another, a theoretical limiting c.d. for alloy deposition was defined as the sum of the two above c.d., and estimated at 257 mA cm^{-2}. Depending on its value the current was applied from 2 to 10 min, and the deposit thickness estimated from Faraday's law, varied from 2 to 20 μm. The electrode potential usually attained a steady value after a few seconds.

4.1. *Aspects of the deposits*

Deposits produced from bath 1, without boric acid, were generally dark. Addition of boric acid allowed more regular deposits and their aspects were usually dull grey; the substrate could not be perfectly covered by deposits with an average thickness below 1 or 2 μm. Deposits of somewhat lighter appearance were produced using the alkaline bath (bath 3); in particular, the surface obtained for middle range c.d. was light grey and semibright, indicating the existence of grains below one micrometer. Figures 3 and 4 compare the aspects of the deposits produced at 24 and 160 mA cm^{-2} from baths 2 and 3.

At the lower c.d., the deposits produced using bath 2 allowed satisfactory coverage of the surface and consisted of granular nodules with a size of the order of 1 μm (Figure 3(a)). The deposit obtained with the alkaline bath was regular, with only a few defects; a close view of the surface (Figure 3(b)) reveals the presence of small alloy grains yielding uniform coverage of the surface.

Deposits formed at the higher c.d. from the acidic bath were observed to consist of large grains with a diameter near 10 μm, and their globular aspect suggested the three-dimensional growth of the alloy (Figure 4(a)). At the same current density, the surface produced from bath 3 was significantly more regular and the crystal size was of the order of 1 μm or below (Figure 4(b)).

4.2. *Nickel contents*

Nickel content in the deposits decreased with increase in the applied cd below 100 mA cm^{-2} and a flat minimum could be observed at 100–120 mA cm^{-2} (Figure 5). Increasing further the current density allowed slight enhancement of the Ni content.

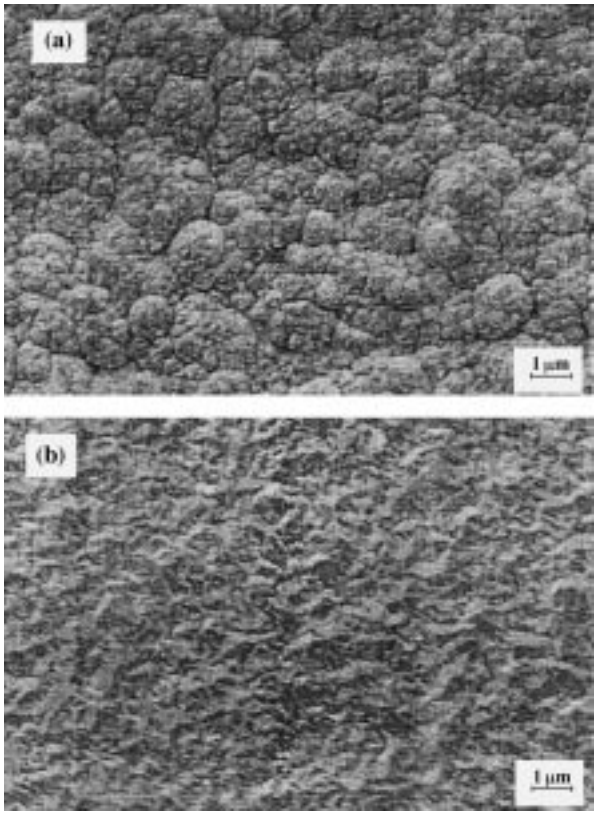

Fig. 3. View of the alloy deposits produced on a RDE at 1000 rpm; $j = 24$ mA cm^{-2} for 640 s. (a) From bath 2; (b) from bath 3.

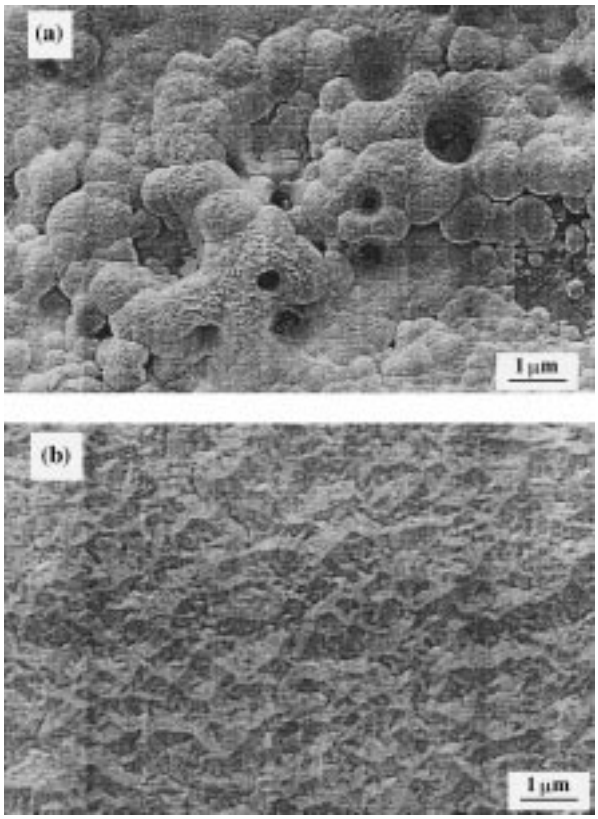

Fig. 4. View of the alloy deposits produced on a RDE at 1000 rpm; $j = 160$ mA cm^{-2} for 120 s. (a) From bath 2; (b) from bath 3.

The nickel content strongly depended on the electrolytic bath (Figure 5). With bath 1, the deposit was relatively nickel poor: its content was near 6% within 1% in the range 70–200 mA cm^{-2}. The presence of boric acid allowed appreciable enhancement of the Ni content, particularly for high current densities: the positive effect of boric acid was previously highlighted [23, 24], and according to Hoare [24], boric acid acts as a homogeneous catalyst and lowers the overvoltage of nickel deposition. Higher Ni contents were obtained from complexing bath 3 whatever the applied current density: in the range 50–200 mA cm^{-2}, the weight content of nickel varied from 12 to 15%. From this Ni-content, these alloys were assumed to consist of δ-phase or of γ- and η-phases mixture; high resistance to corrosion and good mechanical properties of these materials can be expected. Alloys with 17–18% Ni, which roughly corresponds to γ-phase with approximate stoichiometry Ni_5Zn_{21}, could be produced at 250 mA cm^{-2}.

4.3. *Steady-state polarization curves*

Partial current densities for zinc and nickel deposition were calculated from the weight of metal deposited and Faraday's law. Significance of hydrogen evolution was estimated by subtracting these partial c.d.'s from the applied current density. Steady-state current densities were plotted versus the measured electrode potential in Figure 6. The variations of (i/E) curves obtained from baths 1 and 2 were consistent with published data: deposition was observed to start near -1.10 V vs SCE and current densities of the order of the theoretical limiting c.d. of alloy deposition were attained near -1.40 V. The two metals could not be deposited under diffusional control without significant hydrogen evolution. The presence of boric acid resulted in a potential shift near 30 mV towards cathodic polarization. Besides, in addition to its positive effect on Ni deposition, boric acid allowed significant reduction in hydrogen evolution; the negative values reported for i_{H_2} at low polarization of the electrode were likely the fact of uncertainties in estimating the partial current densities which were deduced through chemical analysis and subtraction of partial current densities. In the presence of boric acid, the faradaic yield of alloy deposition was near unity below 100 mA cm^{-2}, and over 85% for higher c.d.'s.

The (i/E) curves obtained from galvanostatic runs from the alkaline bath, were shifted to more cathodic potentials: zinc and nickel deposition started from

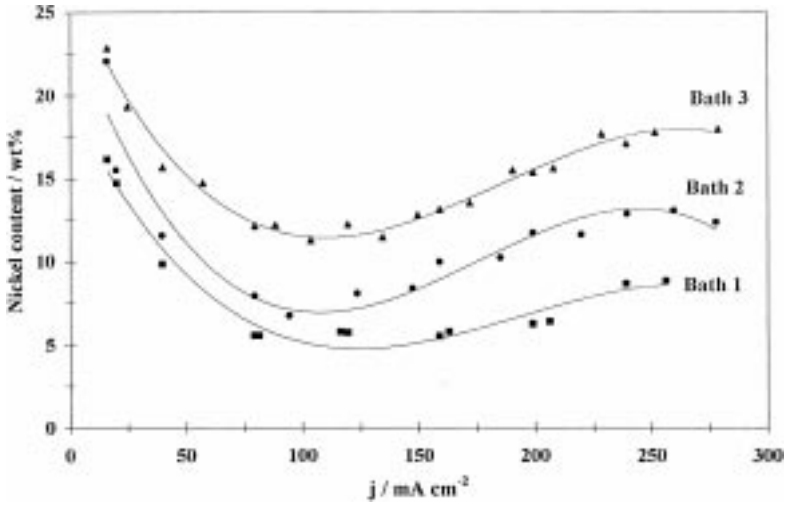

Fig. 5. Nickel content in the alloy deposited against the applied current density; RDE at 1000 rpm.

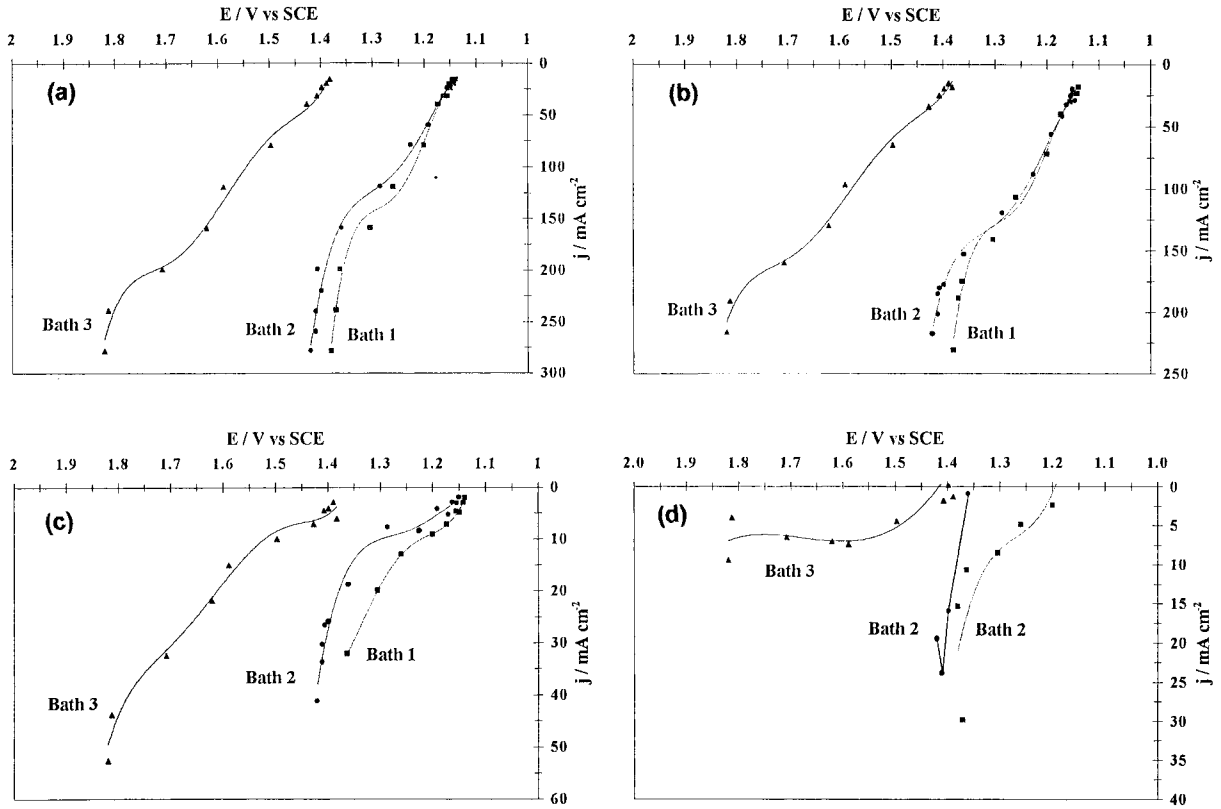

Fig. 6. Steady-state polarization curves obtained on a RDE at 1000 rpm. (a) Global current; (b) Zn deposition; (c) Ni deposition; (d) hydrogen evolution, deduced from the global current and the two metal currents.

−1.38 V, and so did hydrogen evolution. This point is discussed in the following Section.

5. Voltammetric investigations

The electrochemical behaviour of baths 1 and 3 was investigated by cyclic voltammetry. The case of single metal depositions was examined prior to the alloy deposition. The concentration of zinc and nickel chloride were kept at 0.22 and 0.12 mol dm^{-3}, respectively, and the scan rate was fixed at 50 mV s^{-1} for most cases.

5.1. *Nickel deposition*

Voltammetric curves recorded with the acidic bath exhibited a regular increase in the current from −0.5 to −0.9 V, which was attributed to formation of β-Ni [25, 26], with a high hydrogen content. Formation of pure nickel was observed near −1 V before significant hydrogen evolution for higher polarizations (Figure 7). The anodic sweep revealed a small peak near −0.30 V corresponding to dissolution of hydrogen rich β-Ni according to [25, 26], and more significant peaks at +0.08, 0.25, 0.53 and 0.61 V vs SCE, which can be attributed to nickel dissolution. The existence of dissolution peaks at positive potentials was formerly observed by [27], by potentiodynamic stripping of thin nickel deposits.

The deposition peak with ammonia-containing bath were nearly 220 mV more cathodic than with simple nickel baths. The anodic sweep let appear only two peaks: a small peak near −0.48 V which may correspond to dissolution of β-Ni, and a peak of fair intensity at +0.65 V (Figure 7). The displacement of the reduction peaks is discussed as follows.

The presence of $NiOH^+$ was reported by [28, 29] for pH > 4: this species is known to yield adsorbed NiOH intermediate via a first electron transfer. As suggested by Epelboin and Wiart [28], the intermediate reacts with $NiOH^+$ to form metal nickel:

$$NiOH_{ads} + NiOH^+ + 3e^- \rightarrow 2\,Ni + 2\,OH^- \qquad (1)$$

Increasing the pH should favour the formation of $NiOH^+$, even though nickel dihydroxide $Ni(OH)_2$ should predominate, and enhance the production rate of intermediate NiOH at the electrode surface: process (1) is expected to be favoured and nickel deposition should occur at less cathodic potentials. As a matter of fact, complexation of divalent nickel by ammonia is to reduce the concentration of hydroxide $NiOH^+$ and to hinder the formation of NiOH. In addition, the reduction mechanism from ammonia-containing bath can differ significantly from that suggested by [28] and two schemes may be imagined: namely, (i) direct reduction of $Ni(NH_3)_6^{2+}$ complex via one or more electrochemical steps, and (ii) reduction of Ni^{2+} released by decomplex-

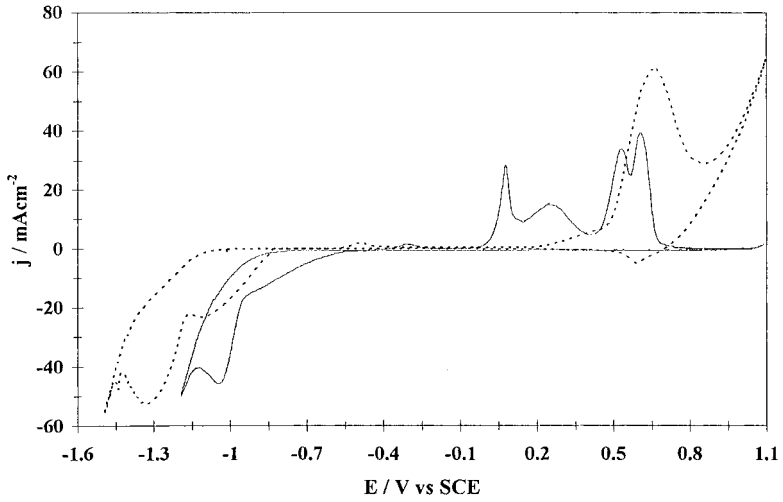

Fig. 7. Voltammetric curves of the nickel system depending on the electrolytic bath; scan rate 50 mV s^{-1}; [$NiCl_2$] = 0.12 mol dm^{-3}. Key: (——) simple nickel bath; (- - - -) ammonia nickel bath.

ation of $Ni(NH_3)_6^{2+}$, this first step being induced by the depletion of the electroactive species near the electrode.

The available experimental data did not permit full understanding of the deposition mechanism; however, the significant shift in potential was not due to the change in pH from 5 to 10 but to the complexing nature of ammonia.

5.2. *Zinc deposition*

Voltammetric curves of zinc deposition and dissolution recorded in the two media exhibited very similar aspects, except for the potential shift near 220 mV towards the cathodic potentials with the ammonia-containing bath (Figure 8). At pH 5 the curves consisted of a cathodic peak near −1.2 V and an anodic peak at −0.92 V, in good agreement with previous works reporting the existence of a peak for zinc dissolution at −0.95 V in chloride media, either at pH 5.6 [27] or at pH 1.6 [30].

Zinc deposition is known to involve adsorbed Zn(I) species and adsorbed hydrogen atom. The deposition mechanism from the ammonia containing bath may be modified by the change in H^+ concentration near the electrode and also by the strong complexation of zinc cations by ammonia.

5.3. *Alloy deposition*

Alloy deposition from the acidic bath started from −1.1 V vs SCE and a cathodic peak was observed near −1.16 V (Figure 9). The anodic sweep recorded at 50 mV s^{-1}, reveals four dissolution peaks at −0.89, −0.70, −0.58 and −0.35 V vs SCE. As reported by other authors [27], [30, 31], the peak at −0.35 V can be attributed to the dissolution of the porous nickel layer. Dissolution of zinc–nickel alloy occurs at more negative potentials than that of pure nickel. According to these authors, the most cathodic peak corresponds to zinc dissolutions from γ- and η-phases of the alloy; the two

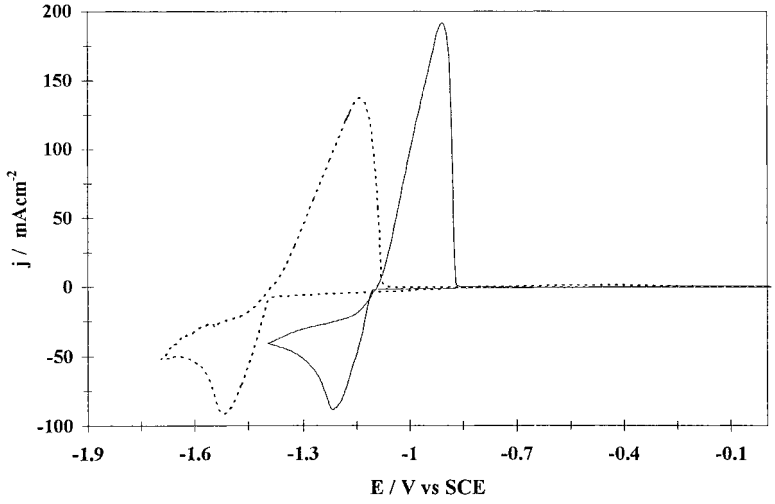

Fig. 8. Voltammetric curves of the zinc system depending on the electrolytic bath; scan rate = 50 mV s^{-1}; [$ZnCl_2$] = 0.22 mol dm^{-3}. Key: (——) simple zinc bath; (- - - -) ammonia zinc bath.

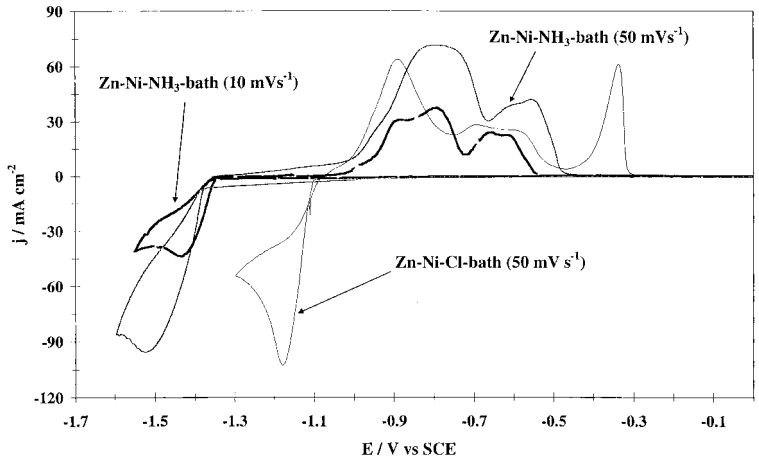

Fig. 9. Voltammetric curves of the zinc–nickel system depending on the electrolytic bath; $[ZnCl_2]$ = 0.22 mol dm^{-3} and $[NiCl_2]$ = 0.12 mol dm^{-3}.

remaining peaks at −0.70 and 0.58 V might be attributed to zinc oxidation from the γ-phase, even though Swathirajan reported the possible dissolution of the nickel-rich α-phase at −0.56 V.

Voltammetric curves of Zn–Ni system in bath 3 were carried out with lower scan rates for the sake of improved resolution of anodic peaks. The positions of the peaks were affected by the scan rate: lowering the rate from 50 to 10 mV s^{-1} resulted in shifts to cathodic potentials near 80 mV (Figure 9). The deposition peak of the alloy from bath 3 was shown to be 300 mV more cathodic than that recorded with the acidic bath. In spite of their moderate resolution, the i/E curves recorded at 10 mV s^{-1}, exhibited four anodic peaks at −0.89, −0.79, −0.65 and −0.61 V (Figure 9); the less cathodic peak may be attributed to Ni dissolution. As for acidic bath 1, the three peaks at fair cathodic potentials may be attributed to successive transitions of the alloy phases by progressive dissolution of zinc: as suggested by [31], δ-phase would be transformed into γ-phase, then into α-phase through successive zinc dissolution steps.

Dissolution was also investigated by potentiodynamic stripping of alloys deposited at 30 and 160 mA cm^{-2} from bath 3, with respective Ni contents near 18% (corresponding to γ-phase) and 12% . The anodic sweep recorded at 5 mV s^{-1} was slightly affected by the Ni content of the deposit (Figure 10), and exhibited three peaks at −0.95, −0.85 and −0.67 V vs SCE. The anodic curves reported in Figures 9 and 10 are fairly consistent and the slight differences in both resolution and position of the peaks may be due to the different techniques used for alloy formation and to the different scan rates. The effect of Ni content in the alloy on the scan was visible only for the less cathodic peak, which was assigned to nickel dissolution (Figure 10): as expected, this peak was more significant for the nickel-richer alloy produced at 30 mA cm^{-2}.

6. Conclusion

The presence of both ammonium ion and ammonia allows buffering of the solution and also strong com-

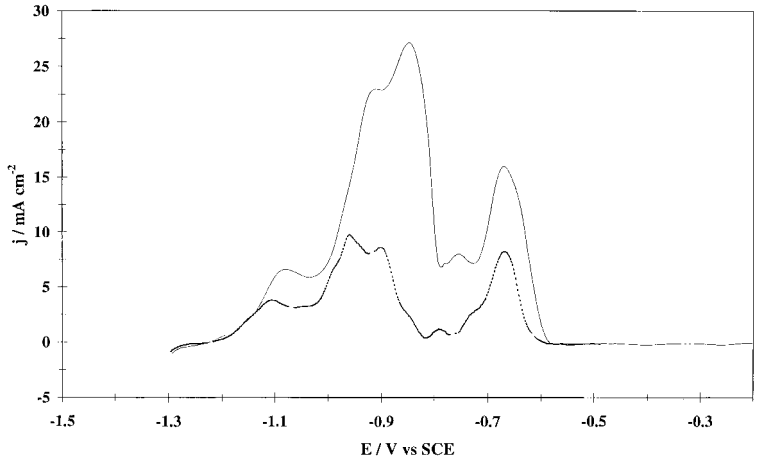

Fig. 10. Potentiodynamic stripping of alloys produced from bath 3 at two current densities: (----) 30 and (——) 180 mA cm^{-2}; scan rate 5 mV s^{-1}.

plexation of the two metal cations. Thermodynamic calculations have shown the predominance of $Zn(NH_3)_4^{2+}$ and $Ni(NH_3)_6^{2+}$ complexes in baths with high ammonia contents and at pH near 10. The electrochemistry of Zn–Ni alloy deposition at pH 10 was investigated in comparison with that from ammonium baths at pH 5, in the presence or not of boric acid. Ni contents in the alloys produced from ammonia-containing baths are 40–60% higher than from regular ammonium baths at pH 5. The deposition of separate metals and Zn–Ni alloys occur at potentials 250 mV more negative than from acidic baths, as shown by galvanostatic experiments and cyclic voltammetry. The potential shift is not due to the change in pH from 5 to 10, but to the complexing nature of ammonia, and the deposition mechanism of the alloy may be affected by the complexation.

Development of ammonia-containing baths for industrial use cannot be envisaged before thorough analysis of the hazards caused by the presence of gaseous ammonia over the electrolytic solution. The analysis should be done taking into account the environmental issues and the available technological solutions: in particular, electrochemical operation conducted under closed atmosphere should limit the toxic gas emission. This aspect is now under investigation.

Acknowledgements

The authors are indebted to the Consejo Nacional de Ciencia y Technologia (Conacyt), Mexico, for the Ph.D grant allocated to I. Rodriguez-Torres.

Appendix

List of symbols

C concentration (mol dm^{-3})
E electrode potential (V vs SCE)
H Henry constant (kg atm mol^{-1})
h salting coefficient (dm^3 mol^{-1})
h_i' salting contribution of ion i (dm^3 mol^{-1})
H_0 Henry constant in pure water (kg atm mol^{-1})
h_G salting coefficient from the volatile species (dm^3 mol^{-1})
I ionic strength (mol dm^{-3} or mol kg^{-1})
I_i contribution of ion i to ionic strength (mol dm^{-3})
j current density (mA cm^{-2})
m molality (mol kg^{-1})
P partial pressure (atm)
P_i partial pressure of gas i (atm)
T temperature (K)
z_i charge number of ion i

Estimation of the partial pressure of ammonia

The gas solubility in liquid can be expressed by Henry's constant, H, linking molality of the molecular solute with its corresponding partial pressure. Assuming fugacity and activity coefficients of ammonia equal to unity leads to the relation:

$$P_{NH_3} = H\, m_{NH_3} \tag{A1}$$

Henry constant is affected by the composition of the electrolyte solution and, in particular, by its ionic strength, I. Setchenow's relation is often used for estimation of Henry constant in electrolyte solutions from its value in pure water, H_0:

$$\log\left(\frac{H}{H_0}\right) = h\, I \tag{A2}$$

where salting coefficient h expresses the effect of the present cations and anions, together with the contribution of the dissolved gas. However, for the present case of multicomponent media, the salting effect was expressed by summing up the contributions of all ions i [32]

$$\log\left(\frac{H}{H_0}\right) = \sum_i h_i' I_i + h_G' \sum_i I_i \tag{A3}$$

where h_i' is the salting contribution of ion i and I_i is its contribution to the ionic strength:

$$I_i = \frac{1}{2} z_i^2 C_i \tag{A4}$$

if z_i denotes the charge of ion i present at C_i. Values of parameters h_i were collected by Onda et al. [33] and are listed below (dm^3 mol^{-1}):

Zn^{2+} −0.059
Ni^{2+} −0.052
NH_4^+ −0.0737
Cl^- 0.3416

whereas h_{NH_3}' is equal to −0.2394 dm^3 mol^{-1} at 25 °C [33]. In the present case, the metal species are under the form of complexes $Zn(NH_3)_4^{2+}$ and $Ni(NH_3)_6^{2+}$, and the actual salting coefficients were considered to be those of free cations. Relation A3 applied to the example of bath 3, yielded a ratio (H/H_0) near 0.578.

Henry's constant of ammonia in pure water was calculated at 25° from the numerical law established by Edwards et al. [34]:

$$\ln H_0 = \frac{-157.552}{T} + 28.1001 \times \ln T - 0.04923\, T - 149.006 \tag{A5}$$

where temperature T is in kelvin. At 25 °C , H_0 equal to of 0.01632 kg atm mol^{-1}. Taking into account the salting effects of the various solutes, Henry's constant H was then estimated at 0.0094 kg atm mol^{-1}.

Besides, the concentration of free ammonia was obtained by subtracting the quantities of ammonia linked to the divalent metal ions from the initial

concentration, 3.4 mol dm^{-3}: the free ammonia concentration was estimated at 1.8 mol dm^{-3}. The partial pressure was deduced from Equation A1, approximating the molality of free ammonia by its concentration in mol dm^{-3}:

$$P_{NH_3} \approx H\, C_{NH_3} = 0.0094 \times 1.8 = 0.01692\,\text{atm}.$$

References

1. G.F. Hsu, *Plat. Surf. Finish.* **71** (1984) 52.
2. V. Raman, M. Pushpavanam, S. Jayakrishnan and B.A. Shenoi, *Metal Finish.* **81** (1983) 85.
3. D.E. Hall, *Plat. Surf. Finish.* **71** (1983) 59.
4. A. Shibuya, T. Kurimoto, K. Korkawa and K. Noji, *Tetso to Hagane* **66** (1980) 771.
5. R. Pfiz and G. Strube, *Trans. Inst. Metal Finish.* **74** (1996) 158.
6. R.G. Baker and C.A. Holden, *Plat. Surf. Finish.* **72** (1985) 54.
7. A. Brenner, *Electrodeposition of Alloys*, vol. 1 and 2, Academic Press, New York (1963).
8. E. Chassaing and R. Wiart, *Electrochim. Acta* **37** (1992) 545.
9. F.J. Fabri-Miranda, O.E. Barcia, O.R. Mattos and R. Wiart, *J. Electrochem. Soc.* **144** (1997) 3441 and 3449.
10. F.J. Fabri-Miranda, O.E. Barcia, S.L. Diaz, O.R. Mattos and R. Wiart, *Electrochim. Acta* **41** (1996) 1041.
11. M.F. Mathias and T.W. Chapman, *J. Electrochem. Soc.* **134** (1987) 574.
12. S.S. Abd El Rehim, E.E. Fouad, S.M. Abd El Wahab and H.H. Hassan, *Electrochim. Acta* **41** (1996) 1413.
13. M. Pushpavanam and K. Balakrishnan, *J. Appl. Electrochem.* **26** (1996) 1065.
14. G. Barcelo, J. Garcia, M. Sarret and C. Müller, *J. Appl. Electrochem.* **24** (1994) 1249.
15. R. Fratesi and G. Roventi, *J. Appl. Electrochem.* **22** (1992) 657.
16. L. Domnikov, *Metal Finish.* **63** (1965) 63.
17. J. Bjerrum, *Metal Amine Formation in Aqueous Solutions*, Ph.D dissertation, Copenhagen (1941); reprinted by P. Haase & Son (1957)
18. S. Kotrly and L. Sucha, *Handbook of Chemical Equilibria in Analytical Chemistry*, Ellis Horwood, Chichester (1985).
19. A. Ringbom *Complexation in Analytical Chemistry*, Interscience Publishers, London (1963).
20. L.G. Sillén and A.E. Martell, *Stability Constants of Metal–Ion Complexes*, Supplement No.1, The Chemical Society, London (1971).
21. H. McConnell and N. Davidson, *J. Am. Chem. Soc.* **72** (1950) 3164.
22. A. Rojas-Hernandez, M.T. Ramirez and I. Gonzales, *Analytica Chim. Acta* **278** (1993) 321.
23. B.V. Tilak, A.S. Gendron and M.A. Mosoiu, *J. Appl. Electrochem.* **7** (1977) 495.
24. J.P. Hoare, *J. Electrochem. Soc.* **133** (1986) 2491.
25. Z. Wu, L. Fedrizzi and P.L. Honora, *Surf. Coat. Technol.* **85** (1996) 170.
26. W.G. Proud, E. Gomez, E. Sarret, E. Valles and C. Müller, *J. Appl. Electrochem.* **25** (1995) 770.
27. F. Elkhabati, G. Barcelo, M. Sarret and C. Müller, *J. Electroanal. Chem.* **419** (1996) 74.
28. I. Epelboin and R. Wiart, *J. Electrochem. Soc.* **118** (1971) 1577.
29. A. Saraby-Reintjes and M. Fleischmann, *Electrochim. Acta* **29** (1984) 557.
30. Y-P. Lin and J.R. Selman, *J. Electrochem. Soc.* **140** (1993) 1299.
31. S.J. Swathirajan, *J. Electrochem. Soc.* **133**, (1986) 671.
32. A. Schumpe, I. Adler and W.D. Deckwer, *Biotechnol. Bioeng.* **20** (1978) 145.
33. K. Onda, E. Sada, T. Kobayashi, S. Kito and K. Ita, *J. Chem. Eng., Japan* **3** (1970) 18.
34. T.J. Edwards, G. Maurer, J. Newman and J.M. Prautnitz, *AIChE. J.* **24**(6) (1978) 966.